


Spontaneous Synchronization and Exceptional Points in Breather Complexes

Wenchao Wang,[†] Zhifan Fang^{✉,†}, Tianhao Xian, Mengjie Zhang, Yang Zhao, and Li Zhan^{✉,*}
State Key Laboratory of Advanced Optical Communication Systems and Networks, School of Physics and Astronomy, Shanghai Jiao Tong University, Shanghai 200240, China

 (Received 9 August 2022; revised 9 June 2023; accepted 3 August 2023; published 24 August 2023)

In this study, we provide an empirical validation of spontaneous synchronization and the exceptional-point- (EP) induced pulse-generation mechanism within the dynamic framework of the breather complex. During the establishment of a nine-breather assembly within a mode-locked fiber laser, we find synchronization in both the breathing frequency and phase. Intriguingly, the formation of these breathers aligns exactly with the junctures where the complex's breathing frequency either diverges from or is entrained into their subharmonics. We posit that such a pulse-generation mechanism is intrinsically associated with the non-Hermitian EPs or the time-translation symmetry breaking. Our in-depth studies into the deconstruction and subsequent reconstruction of mode locking have unveiled a crucial correlation between synchronization and laser stabilization. These findings could stimulate alternative studies, including ultrafast optics, microcavity combs, ocean breather behaviors, non-Hermitian optics, etc.

DOI: [10.1103/PhysRevApplied.20.024060](https://doi.org/10.1103/PhysRevApplied.20.024060)

I. INTRODUCTION

Solitons, an intriguing phenomenon observed in dispersive Kerr media, epitomize the stationary solutions of the nonlinear Schrödinger equation (NLSE) [1]. This fascinating topic has garnered considerable interest across various disciplines such as hydrodynamics [2], biology [3], and marine science [4]. Nonlinearity and the consequential destabilization [5–7] are ceaselessly explored subjects in nonlinear physics, and undoubtedly they are ubiquitous phenomenon in dispersive Kerr media. One oscillation instability of equilibrium called breather soliton has received considerable attention recently [8–17], in which energy concentrates in a localized and oscillatory fashion. Mathematically, they are periodic solutions of NLSE, and physically, they can live in the form of ocean behaviors [8–10] or optical pulsations [11–17]. They are attractive in both practical applications [15–17] and are pivotal in nonlinear science [18]. For instance, they change periodically in both pulse energy and spectral shape, characterized by a breathing frequency f_b , and this added dimension of frequency brings alternative physics.

In 2019, Cole's theory predicted the effect of subharmonic entrainment (SHE) of Kerr breathers [19]. This phenomenon demonstrates that the fineness-dependent f_b can synchronize with the cavity repetition rate f_r in a Kerr resonator. This synchronization creates a frequency-locking plateau of f_b irrelevant to the fineness, and breaks

the continuous time-translation symmetry (TTS [19,20], which is a concept linked to energy conservation according to Noether's theorem [21]). The breaking of TTS has the potential to give rise to another concept known as a "time crystal" [22]. While there is still an ongoing debate on accepting SHE breathers as real-time crystals [23–25], the scientific community generally acknowledges that SHE breathers exhibit time-crystalline signatures [26]. Subsequently, our group conducted experimental verification of this prediction via a mode-locked fiber laser [27]. Additionally, we established numerical and theoretical connections to the exceptional points (EPs) and non-Hermitian optics [28] to further support our findings. Notably, we found that the branching points in the EP theory coincide with the critical points of entering or leaving the SHE state.

On another point, the SHE of breathers can be categorized as a form of generalized synchronization, wherein one harmonic of f_b synchronizes with the cavity frequency f_r . Synchronization is a fundamental concept that occurs widely in the natural world [29–31], wherein different components interact and coordinate to establish a unified rhythm and phase. In scenarios with strong nonlinearity or high gain within the laser cavity, multiple solitons can be generated [32]. The phenomenon of breathing is closely associated with the dynamic loss of stability. Naturally, the presence of breathing or collective instability among multiple pulses is expected in environments characterized by strong nonlinearity. In our subsequent discussions, we refer to these phenomena as "breather complexes." This introduces a multitude of breathing frequencies and sparks other possibilities in terms of physics. For instance, we

*Lizhan@sytu.edu.cn

[†]These authors are contribute equally.

raise questions such as can synchronization or other forms of mutual interaction occur among these multiple breather frequencies? Do such interactions have any implications for laser stabilization? How does the SHE phenomenon influence the behavior of breather complexes? Investigating how these additional frequencies alter the dynamics of the complex is both challenging and crucial.

In this study, we investigate the formation of breather complexes and observe spontaneous synchronization within them, considering both frequency and phase aspects. To track the evolution of the breather complex, we employ the dispersive Fourier transformation (DFT) technique [33], enabling real-time monitoring. Additionally, we integrate the single-shot spectra to analyze the variation in pulse energy. Throughout the formation process, each generated breather originates precisely at the EPs associated with the SHE states of the complex. Furthermore, we introduce changes to the intracavity transmittance in order to disrupt and subsequently rebuild mode locking. As a result, the initially noiselike signals gradually evolve towards regularity and eventually stabilize, accompanied by the synchronization of f_b . We believe that similar underlying mechanisms may be prevalent in various domains, including optical cavities, ocean dynamics, and other relevant fields.

II. SYNCHRONIZATION PHENOMENA OF BREATHER COMPLEXES

A. Conceptual explanation

Here, we focus on the breather complex, which consists of independent breathers with disparate and varied pulse energies within each roundtrip. To illustrate this concept, we present a three-pulse structure in Fig. 1(a), where each pulse is marked by a different color. These breathers exhibit their own breathing modes, as depicted in Fig. 1(b), showing distinct breathing periods and phases. Under normal circumstances, the breathing patterns should keep and operate independently if there is no mutual interaction. But our argument is that they can be synchronized with each other through the spontaneous synchronization effect, embodied in both aspects of phase [see yellow and red cases in Figs. 1(c) and 1(d)] and frequency synchronization [see red and blue cases in Figs. 1(c) and 1(d)]. Finally, this synchronization promotes the initial independent breathing modes to generate a complex with a uniform breathing rhythm.

B. Experimental results

We employed a typical dispersion managed fiber laser [34] to explore the proposed demonstration, as illustrated in Fig. 2(a). The laser is mode locked by the nonlinear polarization rotation (NPR) technique [35], incorporates a 2-m Er-doped fiber (EDF) pumped by a 980-nm laser. For

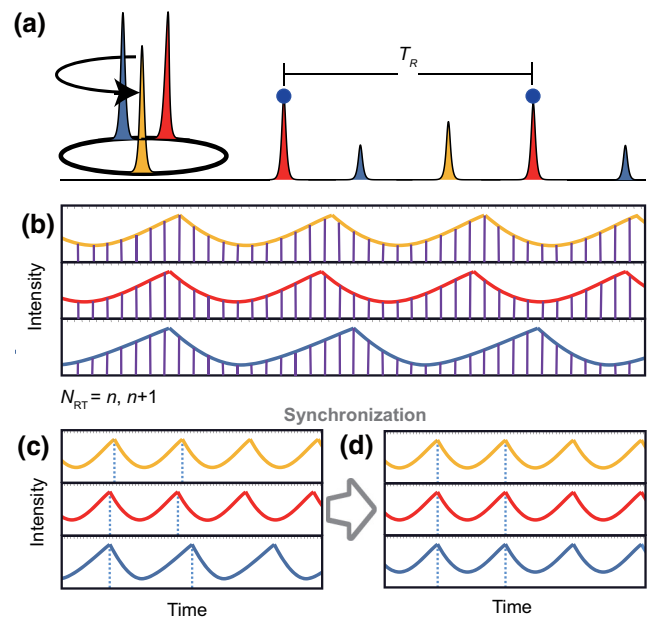


FIG. 1. Conceptual model. (a) The complex state is composed of evolution of three pulses at each roundtrip. (b) Each independently evolved pulse may exhibit breathing behavior at different rhythms, leading to inconsistent phases (as seen in the red and yellow cases), or mismatched frequencies (as seen in the red and blue cases). (c),(d) The mismatches can be eliminated by the spontaneous synchronization effect.

cavity-dispersion management, a 40-cm-long dispersion compensating fiber (DCF) is equipped. The other fibers used are standard single-mode fibers (SMF), resulting in a total cavity length of 7.65 m, corresponding to a repetition rate of 26.92 MHz. The group velocity dispersion values for the DCF, EDF, and SMF at 1550 nm are $65 \text{ ps}^2 \text{ km}^{-1}$, $-48 \text{ ps}^2 \text{ km}^{-1}$, and $-22 \text{ ps}^2 \text{ km}^{-1}$, respectively. To achieve NPR mode locking, a polarization-dependent isolator (PD ISO) and two polarization controllers (PCs) are utilized. To further characterize the complex evolution, we employed two different schemes in the follow-up measurements. Firstly, we directly recorded the transient process by triggering the oscilloscope, which provided evolutionary information in the time domain; secondly, we used the time-stretch scheme, incorporating an extra 2-km-long SMF, as shown in Fig. 2(a). While this scheme could not provide single-shot spectra due to the overlapping of temporal waveforms in multipulse cases, it proved useful for calculating the pulse energy. By integrating the normalized stretched temporal waveform, we can examine how the pulse energy varied during the evolution.

We find a stable complex mode-locking state at the pump power of 600 mW, as shown in Fig. 2(b). The time coordinates are displayed logarithmically to illustrate the oscilloscope trace of the complex. The mode-locking state exhibits a constant breathing period of approximately

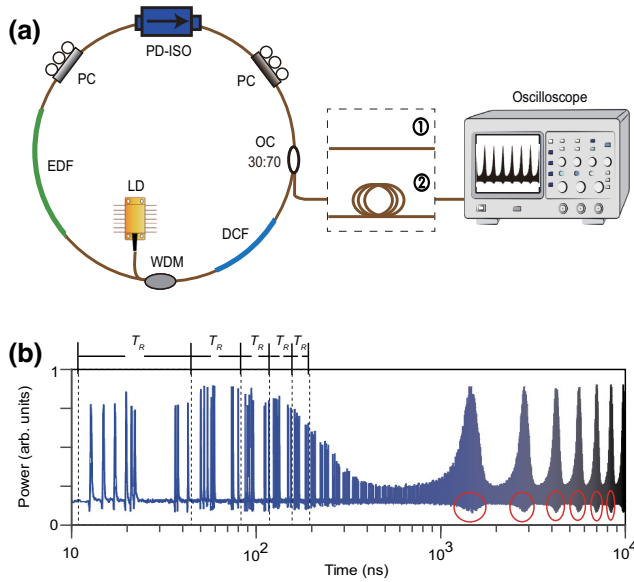


FIG. 2. Experimental setup and breather complex formation. (a) The experimental setup consists of two parts: the mode-locked fiber laser on the left and the direct recording and time-stretch scheme (marked by the serial numbers 1 and 2 correspondingly) for real-time detection on the right. (b) The oscilloscope trace shows the breather complex captured during the experiment.

$\sim 2 \mu\text{s}$, with each roundtrip (RT) containing nine pulses. Although the waveform shape of the complex resembles Q -switched mode locking [36], the breathing period, which is one order of magnitude smaller than the lifetime of the occupied level in Er^{3+} , rules out the possibility of Q switching. The nine-pulse structure supports self-start and can maintain the mode locking for several hours. The conclusion that the complex is composed of breathers is derived not only from the oscillating appearance of the pulse waveform but also from the observation that the minimum intensity occurs at each peak position [indicated by the red marks in Fig. 2(b)]. In breathers or peregrine solitons [18], there are characteristic intensity dips (lower than the background intensity) distributed on both sides of the pulses at each breathing peak.

The breathing period depends on the cavity fineness, which is sensitive to the gain or loss [19]. Initially, the born pulses experience unstable gain since soliton or pulse trains are inspired by modulation instability [1]. As a result, each breather may exhibit varied and unstable breathing periods during the initial stage. However, as observed in the captured nine breathers in Fig. 2(b), they demonstrate a unified breathing rhythm, indicating the presence of synchronization. To further verify this synchronization phenomenon, we tracked the birth of the complex by the first scheme depicted in Fig. 2(a). The recorded time series was segmented based on the roundtrip time and displayed the formation process in Fig. 3. Nine breathers

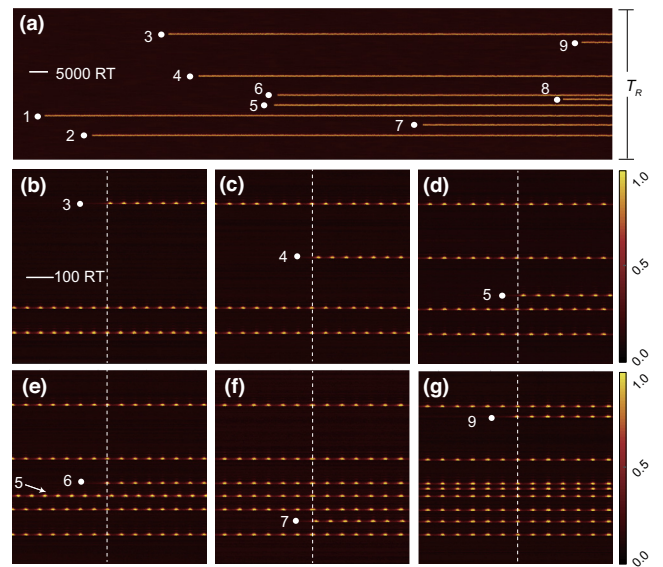


FIG. 3. Phase synchronization. (a) The shot-to-shot build-up process of the nine-breather complex was recorded over a total of 160 000 RTs, with a roundtrip time $T_R = 37.1 \text{ ns}$, corresponding to a repetition rate of 26.92 MHz. (b)–(g) Selected local details are shown, each containing 800 RTs. These details include the cases marked by 3–7, and 9 in (a). The color bar scales the intensity of the temporal waveforms.

emerge one by one, exhibiting similar pulse intensities, but their occurrences of sequence in the time domain appear random, as shown in Fig. 3(a).

C. Phase synchronization

We present six selected local details of the formation process in Figs. 3(b)–3(g) to reveal how synchronization influences the evolution of the breathers. From the diagrams, the breathing periods are close at the initial stages, but the phases of the breathing envelope vary. For instance, in Figs. 3(b)–3(f), the initial phase of each born breather lags behind the rhythm of the entire complex, while in Fig. 3(g) the phase is slightly in advance. However, after hundreds of roundtrips, the breather complex eventually achieves a unified breathing rhythm, regardless of the initially formed phases, thus confirming phase synchronization. The absence of extra nonlinear interactions among the complex is apparent as the movements of each breather remain independent, with no collisions or annihilations observed. We believe the spontaneous synchronization arises from the coupling of breathing modes. These modes are close to each other in both frequency and intensity aspects, and they receive feedbacks from the same cavity. Then the synchronization can spontaneously happen, much like how two asynchronous clocks hanging on the wall will eventually synchronize.

This phenomenon is universal in the real world and can be well explained by the Kuramoto model [37]. The Kuramoto model has proven to be effective in explaining the spontaneous phase synchronization of nonlinear oscillators in many cases of coupled oscillators. In our study, the breather complex exhibits behavior similar to that of coupled oscillating signals in nonlinear oscillators. The breathing envelope of breathers are coupled to each other, much like the intrinsic natural frequency in each single oscillator coupling to all other oscillators. Thus, the breathing phase can be governed by the following equation:

$$\frac{d\theta_i}{dt} = f_b + \frac{K}{N} \sum_{j=1}^N \sin(\theta_j - \theta_i), i = 1, \dots, N, \quad (1)$$

Here the complex comprises N breathers (in this case, $N = 9$), θ_i and θ_j represent the phase of two independent breathers, K is the coupling constant. In this context, Eq. (1) converges only when $\theta_i = \theta_j$, signifying that the breathing behaviors are coupled to one other. As a result, the initial phase deviations are eliminated, leading to synchronization. Consequently, all the breathers eventually achieve phase synchronization during their evolution.

D. Frequency synchronization

We calculated the frequency, denoted as f_b , of each breathing mode during the start-up evolution, as illustrated in Fig. 4(a). To characterize the frequency of each independent breathing mode, we initially separated the breathing

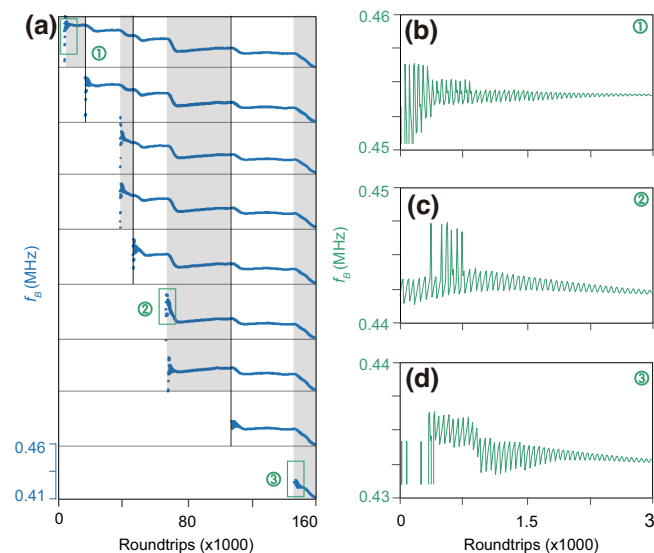


FIG. 4. Frequency synchronization. (a) The breathing frequency variation of each breathing mode during the build-up process. (b)–(d) Local details of the initial oscillatory behavior, corresponding to the green boxes in (a).

modes from the raw oscilloscope waveform data. Subsequently, the precise repetition rate f_r of the signals was acquired using the discrete Fourier transform. The original data were then divided into millions of successive RTs based on f_r , resulting in the shot-to-shot image depicted in Fig. 3. Within each roundtrip, the positions of different breathing modes remained fixed, with each mode occupying approximately eight sampling points (the sampling rate being 10 G sample per second, corresponding to 370 data points in each RT). The calculation of f_b for each breathing mode followed these steps: firstly, we identified the maximum value within these eight effective data points, obtaining an approximate breathing envelope for each mode. Subsequently, with the assistance of the discrete Fourier transform, we determined the exact value of f_b for each breathing mode.

All nine breathers exhibit identical variations in their breathing frequencies, providing strong support for the claim of frequency synchronization. This regularity can be explained through the coupling theory. To illustrate the effect simply, we demonstrate it using a two-frequency model. The coupled equation can be written as follows:

$$\frac{d}{dt} \begin{pmatrix} a_1 \\ a_2 \end{pmatrix} = -2\pi i \begin{pmatrix} f_{b1} & i\eta \\ i\eta & f_{b2} \end{pmatrix} \begin{pmatrix} a_1 \\ a_2 \end{pmatrix}. \quad (2)$$

Here η represents the coupling efficiency, while a_1 and a_2 are the amplitudes of the two breathers, and f_{b1}, f_{b2} denote the breathing frequencies of the respective breathers. The parameter t represents the evolution time. The equation yields eigenvalues of $f_{1,2} = f_{\text{ave}} \pm \sqrt{f_{\text{diff}}^2 - \eta^2}$, with $f_{\text{ave}} = (f_{b1} + f_{b2})/2$ and $f_{\text{diff}} = (f_{b1} - f_{b2})/2$. These eigenvalues represent the frequencies of the two breathers. Therefore, we obtain the relationship $f_1 = f_2 + 2\text{sgn}(f_{\text{diff}})\sqrt{f_{\text{diff}}^2 - \eta^2}$. Notably, when $f_{\text{diff}} < \pm\eta$, the two eigenvalues coalesce, resulting in $f_1 = f_2$. Consequently, if the difference between f_1 and f_2 is small and the coupling effect is stronger than the separate effect caused by the frequency difference, frequency synchronization can be achieved.

Additionally, each time another breather emerges, it results in a decrease in the breathing frequency (f_b) of the other breathers. According to the existing presupposition, f_b relies on the cavity gain, and this gain is sensitive to the pulse energy. The synchronization among the breathers can facilitate a unified f_b , potentially regulating the pulse energy of all nine breathers to be equal. Interestingly, our results also reveal an intriguing phenomenon: the f_b of all generated breathers display the same decayed oscillations during their initial stage. Although the scatter diagram in Fig. 4(a) does not intuitively demonstrate this phenomenon, we provide line diagrams of three selected local details in Figs. 4(b)–4(d), which correspond to the numbered marks in Fig. 4(a). These frequency oscillations should not be attributed to synchronization, as the

pattern has already appeared during the birth of the first breather [Fig. 4(b)]. In this scenario, there are no additional breathing modes present to support synchronization.

III. SUBHARMONIC ENTRAINMENT EFFECT IN BREATHER COMPLEX GENERATION

Such decayed oscillation of f_b always gradually converging to a certain value. We believe the similarity in behavior suggests a common physical origin. One plausible explanation is the SHE effect, which indicates a synchronization between f_b and the cavity frequency f_r . This effect has been shown to have a significant impact in single breather cases. The frequency data acquisition in Fig. 4 is obtained through Fourier transformation, and each value is calculated from a large number of samples, leading to averaged results. To further verify this, we tracked the build-up process using the second scheme depicted in Fig. 2, aiming to reveal the instantaneous frequency by analyzing pulse-energy variations. As shown in Fig. 5(a), the scatter diagram demonstrates the total pulse energy changes within each roundtrip. Notably, each generation of an alternative breather can be distinguished by the presence of nine bulges.

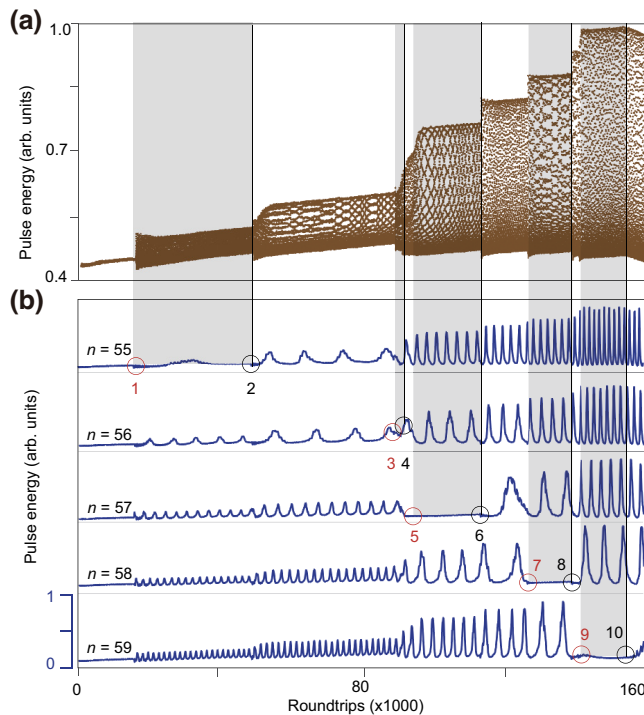


FIG. 5. Experimental verification of the pulse-generation mechanism induced by EP. (a) The variation of pulse energy during the formation process of the complex, calculated by integrating the single-shot spectra. (b) The pulse-energy variation displayed by the down-conversion method.

The line graphs in Fig. 5(b) come from the same original data in Fig. 5(a), the difference is that we draw the diagrams by step m ($m = 55 \sim 59$) RTs. This representation resembles a down-conversion display. By assuming $f_b = mf_r$, the pulse energy in the n -th RT should be approximately equal to that in the $n + m - th$, $n + 2m - th \dots$, $n + km - th$ RT ($k = 3, 4, 5 \dots$). Because taking the abscissa step m RT is equivalent to plotting the curve $y' = \sin(\Delta f T)$, where $\Delta f = f_b - mf_r$, instead of $y = \sin(f_b T)$. In such a display way, once the complex reaches SHE state ($\Delta f = 0$), the energy curve should be almost a straight line, while in cases of non-SHE breathers, $\Delta f \neq 0$, and the energy curve exhibits oscillations with Δf increases as the complex moves farther away from the SHE state.

By comparing Figs. 5(a) and 5(b), we observe that all the breathers are generated precisely at the moment when the complex enters or leaves the SHE state, as indicated by the serial numbers 1 to 9. This observation confirms our conjecture, demonstrating a highly significant correlation between the formation of the breather complex and the SHE effect. It is noteworthy that although no other breathers were produced when leaving the last SHE state [marked by number 10 in the last graph of Fig. 5(b)], the energy of the whole complex starts to decrease, further validating the relevance of the SHE effect in the complex's evolution and stabilization.

In the framework of NLSE modeling, solitons are typically induced by modulation instability [1], arising from certain shaped waves randomly. Consequently, the occurrence of alternative pulses should be inherently stochastic. However, in Fig. 4, the breathers emerge precisely at the EPs, specifically at the critical points of breaking or establishing the complex's SHE state. This indicates that these EPs must significantly alter certain system factors. In response to the principle of "inverse Occam's razor" [38], we just propose potential explanations. Recent studies have shown that EPs in non-Hermitian optics are highly sensitive to disturbances and can be utilized to enhance sensing capabilities [39–41]. It has also been demonstrated that the SHE effect emerges between two EPs, and the SHE breathers are indeed non-Hermitian degenerates [27]. Consequently, energy fluctuations near EPs are amplified, creating a highly unstable background, making it more likely for other pulses to occur. Furthermore, SHE breathers exhibit spontaneous violation of discrete time-translation symmetry (TTS), breaking the TTS. The mainstreams also recognize SHE breathers as having time-crystalline signatures. In this context, the other SHE breathers are constantly produced during the breaking of TTS. It is known that spatial translational symmetry (STS) underlies the formation of crystals and the phase transition from liquid to solid [23]. This leads to the conjecture that the formation of breathers could analogously resemble the STS-promoted crystallization in spatial crystals [42].

IV. LASER STABILIZATION: FROM BREATHER COMPLEX TO MULTIPLE PULSES

Furthermore, we conducted experiments to study the impact of different PC angles on laser stabilization, and the oscilloscope traces were recorded accordingly. The PC angles were adjusted in the same direction, as shown in Figs. 6(a)–6(f), while Figs. 6(g)–6(l) display the corresponding waveforms. Such PC adjustment effectively changes the intracavity transmittance curve, leading to the destruction and reconstruction of mode locking. Of note, synchronization may not always be achieved spontaneously. For example, in Figs. 6(a) and 6(b), the breathers are unsynchronized, resulting in disordered oscilloscope traces in Figs. 6(g) and 6(h). The variation in PC angles alters the transmittance curve and the cavity fineness, leading to different synchronization behaviors in these cases. As discussed in Fig. 5, we suspect that the generation of other breathers should also be related to the EPs or breaking of TTS. The complex becomes synchronized in Fig. 6(c), exhibiting a stable breathing pattern in its waveform [Fig. 6(i)]. Subsequent rotation of the PCs causes a decay in the breathing depth in Figs. 6(d)–6(f), or 6(j)–6(l). The disappearance of the breathing pattern is common in single breather cases (usually achieved by adjusting the pump power). In this instance, the complex loses its breathing properties and eventually stabilizes into multiple pulses

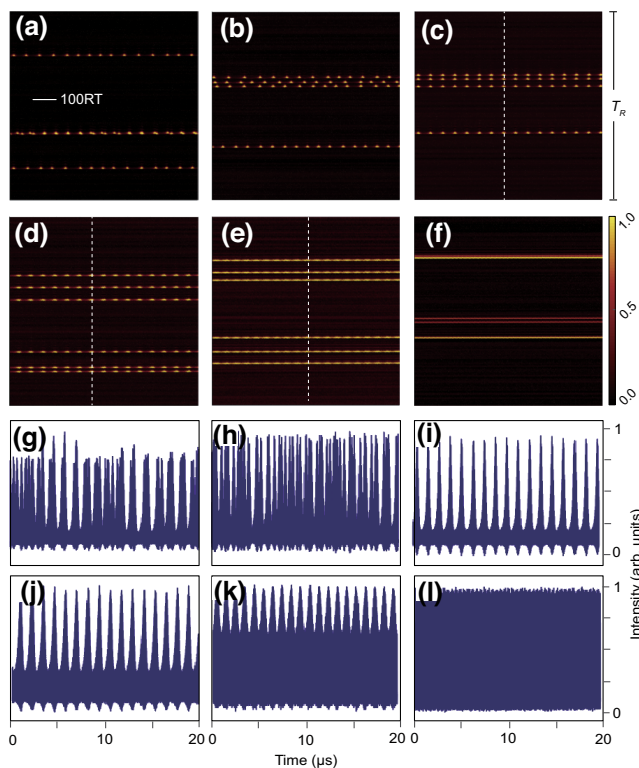


FIG. 6. Experimental results at different PC angles. (a)–(f) Shot-to-shot display. (g)–(l) The corresponding oscilloscope traces.

in Fig. 6(f). It is worth noting that multiple pulses can transition into a stationary single-pulse state, highlighting the relevance of the proposed mechanisms for laser stabilization.

V. CONCLUSION

In conclusion, we report the synchronization and the EP effect in a complex that compose nine breathers by real-time tracking the build-up process. Both the breathing phase and frequency of each formed breathers are spontaneously synchronized by the complex within subsequent hundreds of RTs. Notably, all other breathers were generated exactly when the complex entered or left the SHE state. The initial decayed frequency oscillations of f_b proved compelling evidence of the strong connection between the pulse generation and the SHE effect. We believe that this exotic phenomenon is closely related to the exceptional points effect in non-Hermitian optics, or the TTS breaking. The investigations conducted at different PC angles unveiled that the unsynchronized multiple breathers exhibited chaotic waveforms, while the synchronized complex can be stabilized to multipulses. These revealed mechanisms hold potential implications for various areas, including ultrafast laser, breather dynamics, microresonator, and non-Hermitian optics.

ACKNOWLEDGMENTS

This work was funded by the National Natural Science Foundation of China under Grant No. 11874040, the Foundation for leading talents of Minhang, and the China Postdoctoral Science Foundation under Grant No. 2021M702149.

- [1] G. P. Agrawal *Nonlinear Science at the Dawn of the 21st Century* (Springer, Berlin, Heidelberg, Germany, 2000), p. 195.
- [2] J. Wu, R. Keolian, and I. Rudnick, Observation of a Non-propagating Hydrodynamic Soliton, *Phys. Rev. Lett.* **52**, 1421 (1984).
- [3] N. Akhmediev and A. Ankiewicz, *Dissipative Solitons: From Optics to Biology and Medicine* (Springer Science & Business Media, Berlin, Germany, 2008), Vol. 751.
- [4] J. M. Klymak, R. Pinkel, C.-T. Liu, A. K. Liu, and L. David, Prototypical solitons in the south china sea, *Geophys. Res. Lett.* **33**, L11607 (2006).
- [5] J. E. Marsden and M. McCracken, *The Hopf Bifurcation and Its Applications* (Springer Science & Business Media, Berlin, Germany, 2012), Vol. 19.
- [6] M. R. Guevara, L. Glass, and A. Shrier, Phase locking, period-doubling bifurcations, and irregular dynamics in periodically stimulated cardiac cells, *Science* **214**, 1350 (1981).

- [7] M. Danca, S. Codreanu, and B. Bako, Detailed analysis of a nonlinear prey-predator model, *J. Biol. Phys.* **23**, 11 (1997).
- [8] G.-F. Deng, Y.-T. Gao, C.-C. Ding, and J.-J. Su, Solitons and breather waves for the generalized Konopelchenko-Dubrovsky-Kaup-Kupershmidt system in fluid mechanics, ocean dynamics and plasma physics, *Chaos Solitons Fractals* **140**, 110085 (2020).
- [9] A. Chabchoub, Tracking Breather Dynamics in Irregular Sea State Conditions, *Phys. Rev. Lett.* **117**, 144103 (2016).
- [10] J. Wang, Q. Ma, S. Yan, and A. Chabchoub, Breather Rogue Waves in Random Seas, *Phys. Rev. Appl.* **9**, 014016 (2018).
- [11] T. J. Kippenberg, A. L. Gaeta, M. Lipson, and M. L. Gorodetsky, Dissipative Kerr solitons in optical microresonators, *Science* **361**, eaan8083 (2018).
- [12] T. Herr, V. Brasch, J. D. Jost, C. Y. Wang, N. M. Kondratiev, M. L. Gorodetsky, and T. J. Kippenberg, Temporal solitons in optical microresonators, *Nat. Photonics* **8**, 145 (2014).
- [13] M. Yu, J. K. Jang, Y. Okawachi, A. G. Griffith, K. Luke, S. A. Miller, X. Ji, M. Lipson, and A. L. Gaeta, Breather soliton dynamics in microresonators, *Nat. Commun.* **8**, 1 (2017).
- [14] J. Peng, S. Boscolo, Z. Zhao, and H. Zeng, Breathing dissipative solitons in mode-locked fiber lasers, *Sci. Adv.* **5**, eaax1110 (2019).
- [15] F. Leo, L. Gelens, P. Emplit, M. Haelterman, and S. Coen, Dynamics of one-dimensional Kerr cavity solitons, *Opt. Express* **21**, 9180 (2013).
- [16] J. Peng, Z. Zhao, S. Boscolo, C. Finot, S. Sugavanam, D. Churkin, and H. Zheng, in *Nonlinear Photonics* (Optical Society of America, 2020), p. NpTu3D–2.
- [17] W. Wang, T. Xian, M. Zhang, and L. Zhan, Real-time observation of phase transition of bifurcation evolution in mode-locked lasers, *Opt. Lett.* **47**, 1234 (2022).
- [18] J. M. Dudley, F. Dias, M. Erkintalo, and G. Genty, Instabilities, breathers and rogue waves in optics, *Nat. Photonics* **8**, 755 (2014).
- [19] D. C. Cole and S. B. Papp, Subharmonic Entrainment of Kerr Breather Solitons, *Phys. Rev. Lett.* **123**, 173904 (2019).
- [20] S. B. Papp and D. C. Cole, *Nonlinear Optics* (Optical Society of America, Waikoloa Beach, Hawaii, USA, 2019), p. NTu2A–4.
- [21] W. Sarlet and F. Cantrijn, Generalizations of Noether’s theorem in classical mechanics, *SIAM Rev.* **23**, 467 (1981).
- [22] A. Shapere and F. Wilczek, Classical Time Crystals, *Phys. Rev. Lett.* **109**, 160402 (2012).
- [23] J. Zhang, P. W. Hess, A. Kyprianidis, P. Becker, A. Lee, J. Smith, G. Pagano, I.-D. Potirniche, A. C. Potter, and A. Vishwanath, *et al.*, Observation of a discrete time crystal, *Nature* **543**, 217 (2017).
- [24] H. Keßler, P. Kongkhambut, C. Georges, L. Mathey, J. G. Cosme, and A. Hemmerich, Observation of a Dissipative Time Crystal, *Phys. Rev. Lett.* **127**, 043602 (2021).
- [25] A. Kyprianidis, F. Machado, W. Morong, P. Becker, K. S. Collins, D. V. Else, L. Feng, P. W. Hess, C. Nayak, and G. Pagano, *et al.*, Observation of a prethermal discrete time crystal, *Science* **372**, 1192 (2021).
- [26] D. V. Else, C. Monroe, C. Nayak, and N. Y. Yao, Discrete time crystals, Preprint [ArXiv:1905.13232](https://arxiv.org/abs/1905.13232) (2019).
- [27] T. Xian, L. Zhan, W. Wang, and W. Zhang, Subharmonic Entrainment Breather Solitons in Ultrafast Lasers, *Phys. Rev. Lett.* **125**, 163901 (2020).
- [28] M.-A. Miri and A. Alù, Exceptional points in optics and photonics, *Science* **363**, eaar7709 (2019).
- [29] A. Arenas, A. Díaz-Guilera, J. Kurths, Y. Moreno, and C. Zhou, Synchronization in complex networks, *Phys. Rep.* **469**, 93 (2008).
- [30] S. Boccaletti, J. Kurths, G. Osipov, D. Valladares, and C. Zhou, The synchronization of chaotic systems, *Phys. Rep.* **366**, 1 (2002).
- [31] J. Fell and N. Axmacher, The role of phase synchronization in memory processes, *Nat. Rev. Neurosci.* **12**, 105 (2011).
- [32] Y. Yu, B. Li, X. Wei, Y. Xu, K. K. Tsia, and K. K. Wong, Spectral-temporal dynamics of multipulse mode-locking, *Appl. Phys. Lett.* **110**, 201107 (2017).
- [33] K. Goda and B. Jalali, Dispersive Fourier transformation for fast continuous single-shot measurements, *Nat. Photonics* **7**, 102 (2013).
- [34] B. Oktem, C. Ülgüdür, and F. Ö. Ilday, Soliton–similariton fibre laser, *Nat. Photonics* **4**, 307 (2010).
- [35] H. A. Haus, J. G. Fujimoto, and E. P. Ippen, Structures for additive pulse mode locking, *J. Opt. Soc. Am. B* **8**, 2068 (1991).
- [36] Y.-F. Chen, J.-L. Lee, H.-D. Hsieh, and S.-W. Tsai, Analysis of passively q-switched lasers with simultaneous mode locking, *IEEE J. Quantum Electron.* **38**, 312 (2002).
- [37] J. A. Acebrón, L. L. Bonilla, C. J. P. Vicente, F. Ritort, and R. Spigler, The Kuramoto model: A simple paradigm for synchronization phenomena, *Rev. Mod. Phys.* **77**, 137 (2005).
- [38] I. Mazin, Inverse Occam’s razor, *Nat. Phys.* **18**, 367 (2022).
- [39] H. Hodaei, A. U. Hassan, S. Wittek, H. Garcia-Gracia, R. El-Ganainy, D. N. Christodoulides, and M. Khajavikhan, Enhanced sensitivity at higher-order exceptional points, *Nature* **548**, 187 (2017).
- [40] Y.-H. Lai, Y.-K. Lu, M.-G. Suh, Z. Yuan, and K. Vahala, Observation of the exceptional-point-enhanced Sagnac effect, *Nature* **576**, 65 (2019).
- [41] W. Chen, Ş. Kaya Özdemir, G. Zhao, J. Wiersig, and L. Yang, Exceptional points enhance sensing in an optical microcavity, *Nature* **548**, 192 (2017).
- [42] Y. Zhou, J. Zhang, B. Zhang, L. Qiang, Y. Da, G. Su, and J. Li, Spontaneous symmetry breaking discovers the formation of aeroplane-like ZnO nanocrystals, *Appl. Phys. Lett.* **104**, 121901 (2014).